Intralysosomal Cystine Accumulation in Mice Lacking Cystinosin, the Protein Defective in Cystinosis

Stéphanie Cherqui,[1] Caroline Sevin,[1]† Ghislaine Hamard,[2] Vasiliki Kalatzis,[1] Mireille Sich,[1]
Marie O. Pequignot,[3] Karïn Gogat,[3] Marc Abitbol,[3] Michel Broyer,[1]
Marie-Claire Gubler,[1] and Corinne Antignac[1,4]*

INSERM U423[1] and Department of Genetics,[4] Université René Descartes, Hôpital Necker-Enfants Malades, Plate-forme de Recombinaison Homologue, Institut Cochin-Port-Royal,[2] and CERTO, EA 2502, Université René Descartes, Faculté de Médecine Necker,[3] Paris, France

Cystinosis is an autosomal recessive disorder characterized by an accumulation of intralysosomal cystine. The causative gene, *CTNS*, encodes cystinosin, a seven-transmembrane-domain protein, which we recently showed to be a lysosomal cystine transporter. The most severe and frequent form of cystinosis, the infantile form, appears around 6 to 12 months, with a proximal tubulopathy (de Toni-Debré-Fanconi syndrome) and ocular damage. End-stage renal failure is reached by 10 years of age. Accumulation of cystine in all tissues eventually leads to multisystemic disease. Treatment with cysteamine, which reduces the concentration of intracellular cystine, delays disease progression but has undesirable side effects. We report the first *Ctns* knockout mouse model generated using a promoter trap approach. We replaced the last four *Ctns* exons by an internal ribosome entry site-βgal-neo cassette and showed that the truncated protein was mislocalized and nonfunctional. *Ctns*⁻/⁻ mice accumulated cystine in all organs tested, and cystine crystals, pathognomonic of cystinosis, were observed. *Ctns*⁻/⁻ mice developed ocular changes similar to those observed in affected individuals, bone defects and behavioral anomalies. Interestingly, *Ctns*⁻/⁻ mice did not develop signs of a proximal tubulopathy, or renal failure. A preliminary therapeutic trial using an oral administration of cysteamine was carried out and demonstrated the efficiency of this treatment for cystine clearance in *Ctns*⁻/⁻ mice. This animal model will prove an invaluable and unique tool for testing emerging therapeutics for cystinosis.

Nephropathic cystinosis (MIM 219800) is an autosomal recessive disorder characterized by an intralysosomal accumulation of cystine. The underlying metabolic defect is a defective transport of cystine across the lysosomal membrane (13, 17). Cystine is poorly soluble and forms crystals as its concentration increases. Affected individuals develop a proximal renal tubulopathy (de Toni-Debré-Fanconi syndrome) around 6 to 12 months and progress, if untreated, to end-stage renal failure before the age of 10 years (17). The other main symptoms of nephropathic cystinosis are growth retardation and severe photophobia due to cystine crystal deposits in the cornea. Further clinical signs, such as diabetes, portal hypertension, hypothyroidism, and hypogonadism, as well as muscular and neurological deterioration, subsequently appear due to the accumulation of cystine in all tissues (17). Two other less-severe forms, juvenile and ocular cystinosis, have also been described and have been shown to be allelic by complementation studies (27). The juvenile form (MIM 219900) usually appears between 12 and 15 years, and affected individuals present with photophobia and glomerular renal impairment but not necessarily the Fanconi syndrome (17). The ocular form (MIM 219750) consists solely of a mild photophobia (17). A definitive diagnosis of cystinosis is obtained by assaying for increased intracellular

cystine levels in peripheral blood leukocytes or fibroblasts (28). Cystine levels are directly proportional to disease severity; however, there is substantial overlap between cystine content in patients with all three forms (17). The existing treatment for cystinosis is the drug cysteamine, which cleaves intralysosomal cystine and generates a cystein-cysteamine mixed disulfide that exits lysosomes via the lysine transporter (16). However, the need for regularly spaced doses (four per day) and a number of undesirable side effects, such as digestive intolerance and a persistent nauseating odor, render its administration difficult.

In 1998, we cloned the gene underlying nephropathic cystinosis, *CTNS* (31). *CTNS* mutations were thereafter detected in all forms of the disease, confirming their allelic status (1, 2, 30, 31). *CTNS* is localized to 17p13 and is composed of 12 exons, with the predicted translation start site situated in exon 3 (31). The 2.7-kb *CTNS* transcript encodes a 367-amino-acid protein named cystinosin. Cystinosin is predicted to be a seven-transmembrane-domain (TM) protein, with seven potential N-glycosylation sites in the N-terminal region and a classic tyrosine-based lysosomal targeting signal (GYDQL) in the C-terminal tail (31). We demonstrated that cystinosin is a lysosomal membrane protein and that its correct sorting requires the GYDQL motif and a novel conformational motif, the core of which is YFPQA, situated in the third cytoplasmic loop of the protein (7). Moreover, we recently demonstrated that cystinosin is a lysosomal cystine transporter. Cystinosin is highly specific for L-cystine, and its activity follows Michaelis kinetics and is proton driven (22).

The murine homologue of *CTNS*, *Ctns*, is located on a re-

* Corresponding author. Mailing address: INSERM U423, Hôpital Necker-Enfants Malades, 149, rue de Sèvres, 75015 Paris, France. Phone: (33) 1-44-49-50-98. Fax: (33) 1-44-49-02-90. E-mail: antignac@necker.fr.
† Present address: INSERM U561, Hôpital Saint-Vincent de Paul, 82 avenue Denfert, Rochereau, 75014 Paris, France.

gion of chromosome 11 homologous to human 17p13. *Ctns* consists of 10 exons; it does not contain sequences homologous to the two noncoding exons of *CTNS* (8). The 2.5-kb *Ctns* transcript encodes a 367-amino-acid sequence that is 92.6% similar to cystinosin and contains the seven N-glycosylation sites, seven TM, and two lysosomal targeting signals. In order to progress in the understanding of the pathogenesis of cystinosis and to develop a model system for testing emerging therapeutic possibilities, we created the first mouse model of the disorder by gene targeting in embryonic stem (ES) cells. We report the clinical, histological, and biochemical phenotype of *Ctns* null (*Ctns*$^{-/-}$) mice.

MATERIALS AND METHODS

Targeted disruption of *Ctns* and generation of null mice. A 5-kb *Sal*I *Ctns* fragment beginning in exon 2 and ending in exon 7, and a 2.5-kb *Hin*dIII fragment, containing the 3′untranslated region (UTR) of exon 10 and downstream genomic sequence, were generated from the two genomic clones isolated from the 129/Sv Ev Tac flor DNA genomic library (Stratagene, La Jolla, California) as previously described (8). The *Hin*dIII fragment was subcloned into pBluescript SK(+) (Stratagene) and *Not*I sites were introduced at the two ends by site-directed mutagenesis (QuikChange site-directed mutagenesis kit; Stratagene). The 5-kb *Sal*I and 2.5-kb *Not*I *Ctns* fragments were subsequently subcloned into the plasmid S35 (32), 5′ and 3′ to the internal ribosome entry site (IRES)-β*gal-neo* cassette, respectively. The resulting targeting vector was purified on a CsCl gradient and linearized by *Xho*I digestion, prior to electroporation of ES cells from 129 Sv mice (34); the endogenous *Ctns* expression of the ES cells was verified by Northern blot analysis. Transformants were selected with G418 (250 μg/ml). Recombinant ES cells, assayed by Southern blot analysis, were microinjected into C57BL/6 blastocysts, which were then reimplanted in pseudopregnant B6CBA females to generate chimeric mice that were intercrossed with C57BL/6 females. The agouti-colored offspring were genotyped to select for heterozygotes. DNA was extracted from tail samples of these mice using the DNA Now kit (Biogentex, Houston, Tex.) and was amplified by 30 PCR cycles of 1 min at 94°C, 1 min at 55°C, and 1 min at 72°C using the following three primers: GT10F 1 (5′-GATCTTCGGAGACCCAACC-3′) situated in the open reading frame (ORF) of exon 10, GTgalF (5′-TCCAGCGGGGGGATCTCATGT-3′) in the β*gal-neo* cassette, and GT10R (5′-CAGGGCAGCTTACTGATTGA-3′) in the 3′ UTR of exon 10. Amplification resulted in products of 1,085 bp for the wild-type allele and 700 bp for the recombinant allele. Heterozygous offspring were intercrossed to produce *Ctns*$^{+/+}$, *Ctns*$^{+/-}$, and *Ctns*$^{-/-}$ experimental mice, which were tested for the correct disruption of *Ctns* by Southern and Northern blot analyses. Animals were handled in accordance with all national guidelines and institutional policies.

***Ctns* expression pattern. (i) X-Gal (5-bromo-4-chloro-3-indolyl-β-D-galactopyranoside) staining.** Dissected tissues from *Ctns*$^{+/+}$ and *Ctns*$^{-/-}$ mice (age range, postnatal day 0 to 10) were fixed in phosphate-buffered saline (PBS) containing 4% paraformaldehyde at room temperature for 30 min. β-Galactosidase activity was detected by incubation in a staining solution as described previously (20).

(ii) RT-PCR. Total RNA was isolated from the kidney, brain, and muscle of a 1-month-old *Ctns*$^{+/+}$ mouse using the RNAeasy mini kit (Qiagen, Courtaboeuf, France). cDNA synthesis was carried out with the SuperScript Choice System kit (Invitrogen, Life Technologies, Breda, The Netherlands) using 500 ng of RNA from each tissue and random hexamers. Reverse transcription (RT)-PCR amplification was subsequently performed by 30 cycles of 1 min at 94°C, 1 min at 55°C, and 1 min at 72°C using the following *Ctns* cDNA primers: RT5F (5′-CCGGTTCTTGGTGATACACA-3′) in exon 5 and RT10R (5′-CCGAACTTGGTTGGGTCT-3′) in exon 10.

Subcellular localization and functional analysis of wild-type and truncated *Ctns*-encoded proteins. The entire *Ctns* ORF was amplified using the forward primer 5′-TTCTGAGAAGTCAGAGACCATGAGG-3′, situated at the start of exon 1, and the reverse primer 5′-TGTGTGCCAGCTGCTTCTCT3′, situated in the 3′ UTR. The truncated *Ctns* ORF from exons 1 to 7 was amplified using the same forward primer coupled with the reverse primer 5′-GTCGACGGGGTTC ACACCAT-3′, situated at the *Sal*I site (position 620). The two PCR products were independently subcloned into the PGEM T-easy vector (Promega, Madison, Wis.). The entire and the truncated *Ctns* ORF inserts were subsequently excised by *Eco*RI digestion and reintroduced into the expression vectors pEGFP-N1 (Clontech, Palo Alto, Calif.), in-frame with the *GFP* cDNA se-

quence, generating the fusion constructs pCtns-EGFP and pΔCtns-EGFP, respectively, and pcDNA3.1/Zeo+ (Invitrogen, Paisley, United Kingdom), generating the constructs pcDNA-Ctns and pcDNA-ΔCtns, respectively. Site-directed mutagenesis was used to modify pcDNA-Ctns to generate a construct carrying a deletion of the C-terminal lysosomal sorting motif GYDQL (pcDNA-Ctns-ΔGY-DQL). The pCtns- and pΔCtns-EGFP fusion constructs were transiently transfected into MDCK cells, and the subcellular localization of the fusion proteins were analyzed as previously described (7). To study the cystine transport function, the pcDNA-Ctns, -Ctns-ΔGYDQL, and -ΔCtns expression constructs were transiently transfected into COS-7 cells, and cystine uptake was studied at neutral and acid pHs as previously described (22).

Characterization of *Ctns*$^{-/-}$ mice. (i) Cystine assay. Dissected tissues were immediately homogenized in 750 μl of *N*-ethylmaleide (650 μg/ml; Sigma, St. Louis, Mo.) in PBS. Proteins were precipitated by the addition of 300 μl of 15% sulfosalicylic acid. The protein pellet was then diluted in 1.5 ml of 0.1 N NaOH, and protein content was determined by the Lowry method (23). Cystine content was assayed by radiocompetition with ^{14}C-cystine for the cystine-binding protein (CBP; Riverside Scientific Enterprises, Bainbridge Island, Wash.) as previously described (25).

(ii) Histological analysis. For light microscopy, tissues from 25 *Ctns*$^{-/-}$ mice (from 4 to 78 weeks old) were fixed in 15% formalin and embedded in paraffin. Sections were stained with hematoxylin and eosin, trichrome light green, and periodic acid with hematoxylin. Sections unstained or briefly stained with methylene blue in absolute alcohol were used for the detection of cystine crystals. Tibias from six *Ctns*$^{-/-}$ mice (12 to 18 months old) were fixed in formalin, decalcified 8 days in 10% EDTA, and embedded in paraffin. Sections were examined on a Leitz Orthoplan microscope (Leica Microscopic Systems). For electron microscopy, tissues from six *Ctns*$^{-/-}$ mice (24, 35, or 52 weeks old) were fixed in 2.5% glutaraldehyde–0.2 M cacodylate buffer–PBS (pH 7.4) for 24 h at 4°C and postfixed in 2% osmium tetraoxide for 1 h at room temperature. Alternatively, specimens from two mice were directly fixed in osmium tetraoxide for the visualization of dark cells (29). Fixed specimens were embedded in epoxy resin (Epon 812; Polysciences, Warrington, Pa). Semithin sections for light microscopy (1 μm) were stained with toluidine blue. Ultrathin sections (70 Å) were stained with uranyl acetate-lead citrate and examined with a Zeiss EM 902 electron microscope. Tissue specimens from littermate controls (*Ctns*$^{+/+}$ or *Ctns*$^{+/-}$) were systematically processed and examined under the same conditions.

(iii) Plasma and urine analyses. Blood was collected by cardiac puncture of anesthetized mice. Urine was either collected directly or after 24 h in a metabolic cage. Plasma and urine electrolytes, creatinine, alkaline phosphatase, uric acid, and creatine phospho-kinase (CPK) levels were assayed on a Hitachi (Tokyo, Japan) model 917 automatic analyzer. Urine amino acids levels were determined by ion exchange chromatography in an Aminotac amino acid analyzer (JEOL Ltd., Welwyn Garden City, United Kingdom). Plasma-free triiodothyronin (FT3) and thyroxin (FT4) levels were determined by FT3 DYNOtest (Brahms, Henningsdorf, Germany) and radioimmunoassay (kit from Immunotech, Beckman Coulter Inc., Miami, Fla.), respectively.

(iv) Behavioral testing. Behavioral tests were carried out on mice that were 7 to 13 months old. For the actimeter test, mice were placed in empty cages for 3 h and their vertical and horizontal movements were recorded by four infrared sensors (Immetronic, Bordeaux, France). Motor activity was expressed as the total number of times the infrared beams were crossed. For the open-field test, mice were placed in an enclosure (100 by 100 cm) divided into 20-by-20-cm squares for a 9-min period. The number of times a square was crossed in the outer or inner ring and the number of rearing behaviors were recorded (9).

(v) Ocular and bone examination. The eye function of four *Ctns*$^{-/-}$ mice and two control C57BL/6 mice, all 8 months of age, was tested. The mice were dark-adapted for 12 h and anesthetized. The pupils were dilated with 10% phenylephrine hypochloride and 0.5% tropicamide. Electroretinograms (ERG) were recorded from the anesthetized (0.4% oxybuprocaine hydrochloride) corneal surface using methods described previously (26). A gold-ring electrode made contact with the cornea through a layer of 1.3% hydroxyethyl cellulose. Needle electrodes placed in the cheek and tail served as reference and ground leads, respectively. The scotopic and photopic ERG responses were recorded in a Nicolet Ganzfeld (Nicolet, Madison, Wis.). Images of the cornea and retina were taken using a photographic slit lamp (Topcon SL 8Z) and a 20-diopter Volk lens. X-ray examination of the entire skeleton was performed on anesthetized mice with identical radiation energies (45 kV, 1.2 mA) and exposure times (3 ms).

Statistical analysis. All data were analyzed for a statistically significant difference between *Ctns*$^{+/+}$, *Ctns*$^{+/-}$, and *Ctns*$^{-/-}$ mice, using one-way analysis of
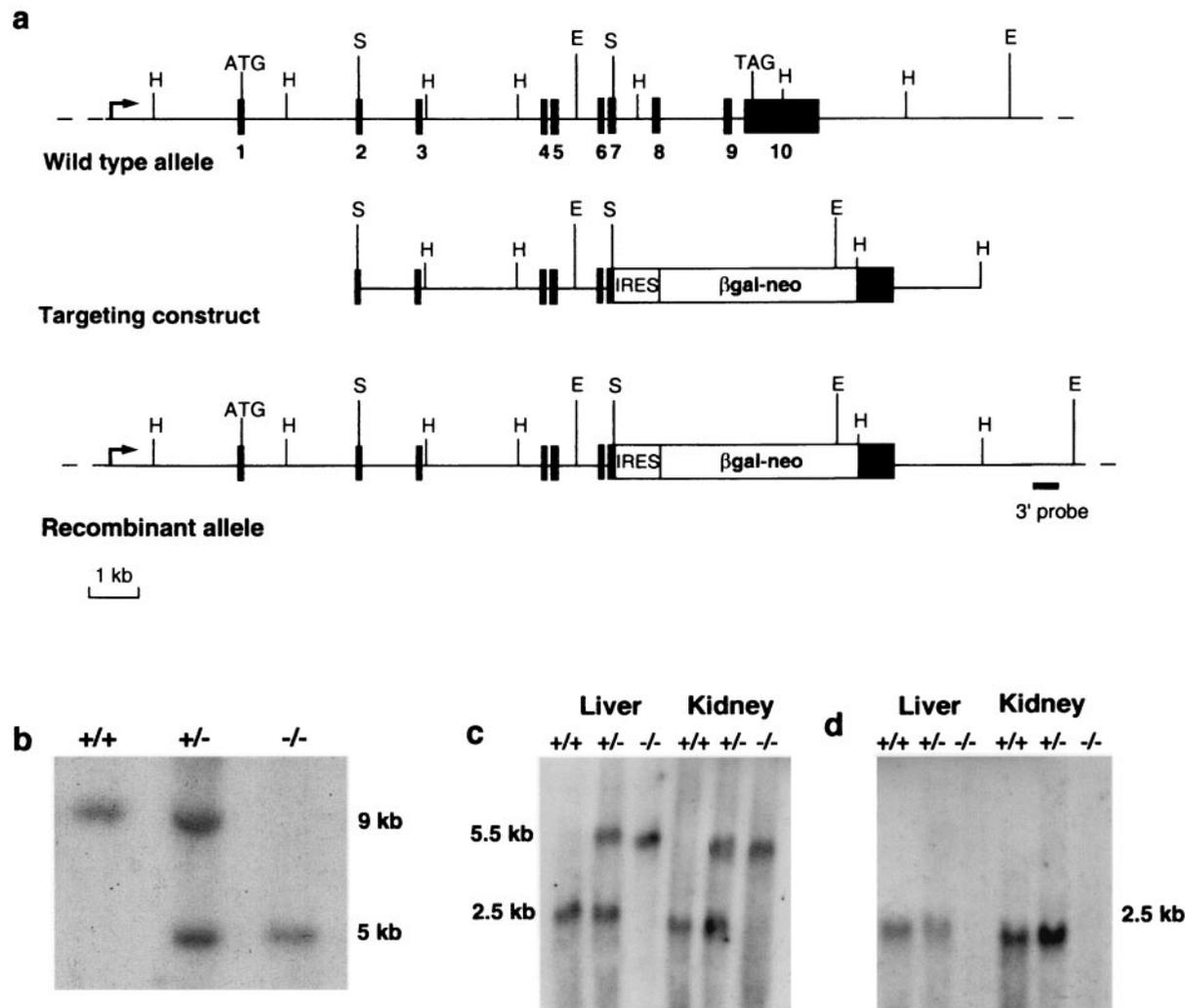
FIG. 1. Disruption of the *Ctns* gene. (a) Schematic representation of the genomic structure of the wild-type murine *Ctns* gene (top), the targeting construct (middle), and the recombinant allele (bottom). The 10 exons are represented by black boxes. *Hin*dIII, *Sal*I, and *Eco*RV restriction sites are indicated by H, S, and E, respectively. The region from exon 7 to the stop codon of exon 10 of the *Ctns* gene was replaced by an IRES-β*gal-neo* cassette; this recombinant gene is under the control of the endogenous *Ctns* promoter (arrow). (b) Southern blot analysis of *Eco*RV-digested genomic DNA from *Ctns*$^{+/+}$, *Ctns*$^{+/-}$, and *Ctns*$^{-/-}$ mice, using a probe located 3′ to the targeting construct (solid bar). The endogenous ~9-kb band was detected in the *Ctns*$^{+/+}$ mice; the recombinant ~5-kb band, created due to the presence of an *Eco*RV site in the cassette, was detected in the *Ctns*$^{-/-}$ mice; and both bands were detected in the *Ctns*$^{+/-}$ mice. (c) Northern blot analysis of 20 μg (total) of liver and kidney RNA from *Ctns*$^{+/+}$, *Ctns*$^{+/-}$, and *Ctns*$^{-/-}$ mice, hybridized with a 5′ probe spanning *Ctns* exons 1 to 3. The endogenous 2.5-kb *Ctns* transcript was detected in the *Ctns*$^{+/+}$ mice; a larger ~5.5-kb transcript, corresponding to the fusion of the remaining *Ctns* exons and the β*gal-neo* transcript, was detected in *Ctns*$^{-/-}$ mice; and both transcripts were detected in *Ctns*$^{+/-}$ mice. (d) The same Northern blot hybridized with a 3′ probe spanning exon 10. The 2.5-kb *Ctns* transcript was detected in *Ctns*$^{+/+}$ and *Ctns*$^{+/-}$ mice, whereas no band could be seen in the *Ctns*$^{-/-}$ mouse.

variance followed by Fisher protected least-significant-difference post hoc analysis. Results are expressed as the mean ± standard error of the mean (SEM). A *P* of 0.05 was required for a difference to be considered as significant.

RESULTS

Generation of *Ctns*$^{-/-}$ mice. We verified that *Ctns* was endogenously expressed in ES cells by Northern blot analysis (data not shown), allowing us to use a "promoter trap" approach (32) to inactivate the *Ctns* gene. We replaced the last four exons of the murine *Ctns* gene by an IRES-β*gal-neo* cassette, by homologous recombination (Fig. 1a). Two correctly targeted ES clones were used to establish germ line chimeras

and their heterozygous offspring (*Ctns*$^{+/-}$). The correct inactivation of *Ctns* was verified by Southern blot and Northern blot analyses (Fig. 1b to d).

In the absence of available antibodies, the lack of functional protein encoded by the recombinant allele was verified by subcellular localization and functional studies (Fig. 2a and b). Wild-type murine cystinosin shared the same characteristics as human cystinosin; i.e., it was localized to lysosomes and transported cystine at acidic pH. In contrast, the truncated murine cystinosin was mislocalized to the plasma membrane and had lost its cystine transport function. These results confirm that murine cystinosin is a lysosomal cystine transporter and that
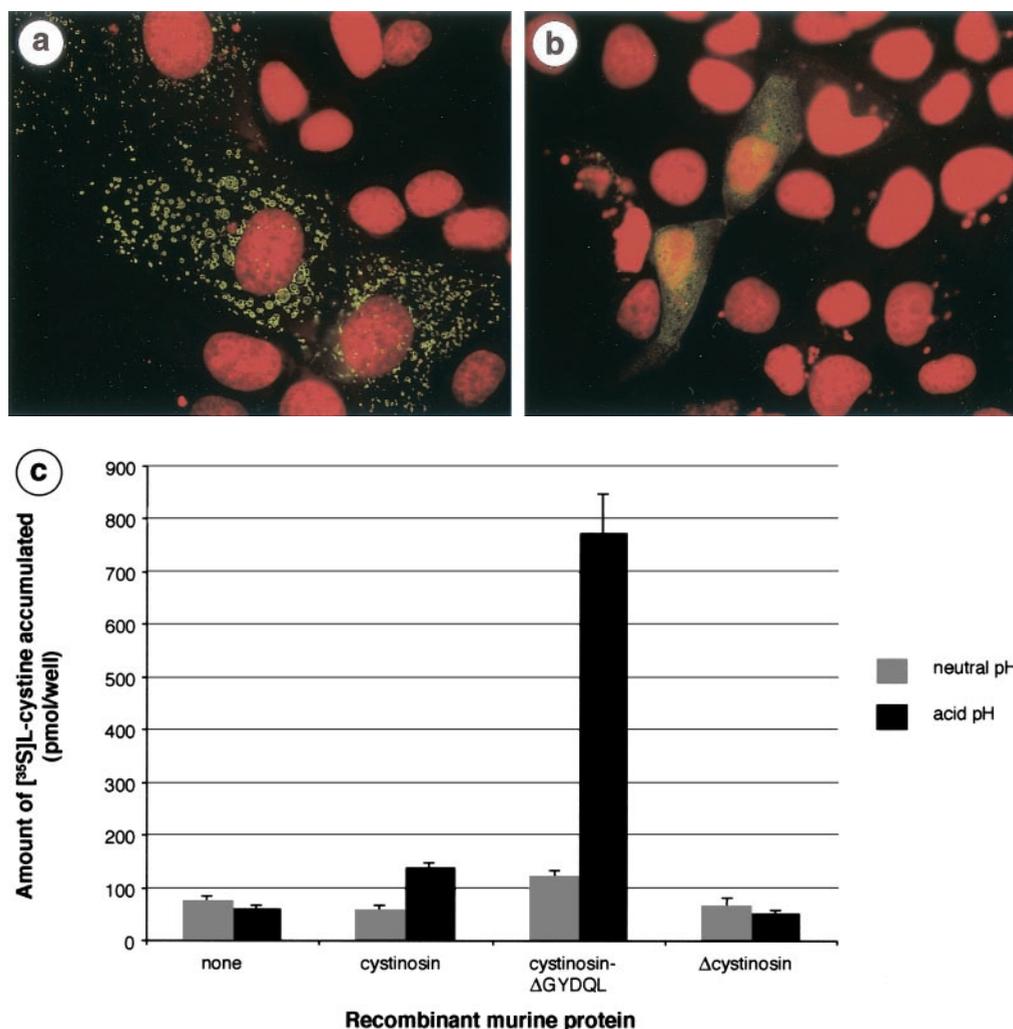
FIG. 2. Subcellular localization and cystine uptake ability of wild-type and truncated murine cystinosin. (a) MDCK cells transiently transfected with the pCtns-EGFP construct. The nucleus, labeled with propidium iodide, is shown in red, and the fluorescent signal from the cystinosin-green fluorescent protein (GFP) fusion protein is localized to the lysosomes. (b) MDCK cells transiently transfected with pΔCtns-EGFP. Δcystinosin-GFP is localized to the plasma membrane. No fluorescent signal is observed in the lysosomes. (c) Functional studies required the targeting of murine cystinosin to the plasma membrane, which is achieved by deleting the C-terminal lysosomal targeting motif GYDQL. Assay of transfected cells for ^{35}S-cystine uptake is performed in a neutral (pH 7.4 [gray bars]) or acidic (pH 5.6 [black bars]) extracellular medium. At neutral pH, cells expressing cystinosin-ΔGYDQL show a modest increase in the amount of accumulated ^{35}S-cystine compared to mock-transfected cells or wild-type cystinosin-expressing cells. At acid pH, a dramatic increase in accumulated ^{35}S-cystine is observed in cystinosin-ΔGYDQL-expressing cells but not in mock-transfected cells. Also at this pH, a small amount of ^{35}S-cystine is taken up by wild-type cystinosin-expressing cells, consistent with the faint signal obtained for the wild-type protein occasionally seen at the plasma membrane. In contrast, accumulated cystine levels are equivalent to background at both neutral and acid pHs for the Δcystinosin-expressing cells. Solid bars correspond to the means of four assays. Error bars correspond to SEM.

the truncated protein produced by the $Ctns^{-/-}$ mice, if stable, is nonfunctional.

As an internal control for the construct, we checked the expression of the β*gal* gene under the control of the endogenous *Ctns* promoter in newborn $Ctns^{-/-}$ mice compared to their wild-type littermates. No blue staining was detected in any of the organs of the $Ctns^{+/+}$ mice, whereas a β*gal* expression was detected in all organs of the $Ctns^{-/-}$ mice, with the exception of muscle (data not shown). We previously demonstrated that no *Ctns* transcript could be detected in skeletal muscle by Northern blot analysis (8). By RT-PCR amplification of muscle, kidney, and brain RNA, from a wild-type

mouse using *Ctns* specific cDNA primers, a faint band of the expected size (671 bp) was detected in muscle, and a stronger band was detected in kidney and brain (data not shown). Altogether, these data suggest a weak *Ctns* expression in muscle, thereby accounting for the lack of detectable β*gal* expression in this tissue.

Phenotype of $Ctns^{-/-}$ mice. The $Ctns^{+/-}$ mice were subsequently intercrossed to obtain $Ctns^{+/+}$, $Ctns^{+/-}$, and $Ctns^{-/-}$ mice. Of 133 offspring, 48% were female and 52% were male. Mice were systematically genotyped by PCR amplification of tail DNA (see Materials and Methods), showing that 25.6% were $Ctns^{+/+}$, 41.7% were $Ctns^{+/-}$, and 32.7% were $Ctns^{-/-}$,

consistent with a classic Mendelian segregation and an absence of prenatal mortality for the null mice. Moreover, the $Ctns^{-/-}$ mice demonstrated normal growth, development, and fertility but presented biochemical, histological, and clinical abnormalities.

Cystine accumulation. Intracellular cystine content of different organs from $Ctns^{+/+}$, $Ctns^{+/-}$, and $Ctns^{-/-}$ mice from birth to 1 year of age was assayed by radiocompetition. In total, 161 assays (71 $Ctns^{+/+}$, 21 $Ctns^{+/-}$, and 69 $Ctns^{-/-}$) were performed. Cystine content was significantly increased in $Ctns^{-/-}$ mice in comparison to $Ctns^{+/+}$ mice (22.5 ± 4.3 versus 0.55 ± 0.13 nmol of half-cystine/mg of protein; $P < 0.0001$). (Fig. 3a). The cystine content of $Ctns^{+/-}$ mice was similar to that of the $Ctns^{+/+}$ mice (0.22 ± 0.12 nmol of half-cystine/mg of protein). Cystine accumulation was clearly observed in all organs tested with the highest levels consistently seen in liver and the lowest in brain (Fig. 3a). This accumulation was present from birth and increased with age (Fig. 3b). An assay of the cystine content of whole embryonic day 13.5 $Ctns^{-/-}$ embryos showed an accumulation compared to $Ctns^{+/+}$ embryos (1.28 ± 0.14 versus 0.09 ± 0.01 nmol of half-cystine/mg of protein; $P=0.0009$).

Histology. The main pathological finding was the observation of cystine crystals. They were rectangular, hexagonal, or elongated in form and strongly birefringent by polarization or phase-contrast microscopy (Fig. 4a). They were first observed in a 24-week-old mouse. At this age, they were rare, being detected in interstitial cells of various organs (testis, thyroid, salivary glands, lymph nodes) and in some Küppfer cells, and a few being detected in proximal tubular cells.

During the course of evolution, cystine crystal deposition remained absent, mild or moderate according to age and tissue. Within the liver, in 35 weeks old mice, crystal accumulation was irregular in Küppfer cells and absent in hepatocytes (Fig. 4b). Numerous Küppfer cells were dark after osmium fixation (Fig. 4c), forming dark cells which are unique to cystinosis (29). By electron microscopy, crystals appeared as empty angular structures, usually limited by a single unit membrane or located within dark lysosomes (Fig. 4d). Findings were similar in older mice, without any significant increase in crystal deposition. At 35 weeks, in the kidney, crystals appeared as black spindles after osmium fixation (Fig. 4e). Isolated or small groups of proximal tubular cells were vacuolized (Fig. 4f). Vacuoles were identified as swollen mitochondria (Fig. 4g). However, most proximal tubules appeared normal as well as distal tubules, glomeruli and interstitium (Fig. 4h). No progression of the renal lesions was observed in older mice, whereas cystine crystals accumulated progressively within capsular interstitial cells. In the eye, at 35 weeks of age, cystine crystals were present within the melanocytes of the conjunctiva and in choroidal and scleral interstitial cells (Fig. 4i). This distribution persisted in older mice. Rare crystals were detected in the cornea but not in the retina, the structure of which remained normal.

Cystine crystals were seen in the skeletal muscle of a 1-year-old mouse with severe clinical muscular impairment. They were located in interstitial cells and not in myocytes (Fig. 4j) and very focally associated with myocyte necrosis. Surprisingly, no abnormality was detected in three other mice of the same age or older. However, in the same mice, crystals were abundant in the heart (Fig. 4k and l) and in the interstitial cells but not in the myocytes. They were observed in the interstitial cells of the thyroid, pancreas, ovaries, uterus, testis, and salivary glands but not in the corresponding epithelia. They were present in the spleen and lymph nodes. None of these organs showed obvious signs of structural abnormalities. Crystals were not detected in the lungs, brain or spinal cord of any mice regardless of age. No cystine crystal accumulation was seen in $Ctns^{+/-}$ mice.

Biochemistry. In a follow-up lasting 1.5 years, $Ctns^{-/-}$ mice did not reveal any clinical or biological signs of a tubulopathy nor renal failure. Plasma analyses performed on 25 $Ctns^{+/+}$ and 62 $Ctns^{-/-}$ mice showed no significant difference in creatinine, urea, bicarbonatemia, uric acid, calcium, phosphate, or alkaline phosphatase levels. Urine analyses showed no significant difference for proteinuria, glycosuria, phosphaturia, calciuria, or aminoaciduria between $Ctns^{-/-}$ ($n = 52$) and $Ctns^{+/+}$ ($n = 29$) mice (data not shown). Furthermore, $Ctns^{-/-}$ mice did not present with biological signs of diabetes, as measured by glycemia, or hypothyroidism, as measured by FT4 and FT3 levels (data not shown).

Behavior. At 6 to 8 months of age, the wild-type and $Ctns^{-/-}$ mice exhibited behavioral differences, with the latter being less active. Behavioral studies were hence performed on older mice (ages, 7 to 13 months) in actimeter and open-field apparatuses, which analyze, respectively, locomotive activity in a familiar environment and exploratory behavior. For the actimeter test, the number of times a mouse moved did not differ between null ($n = 8$) and wild-type ($n = 8$) mice (41.1 ± 11.2 versus 42.4 ± 9.8; $P > 0.05$). The number of rearing behaviors was lower in $Ctns^{-/-}$ mice than in $Ctns^{+/+}$ mice, but the difference did not reach significance (82 ± 25.2 versus 126.7 ± 24.9; $P > 0.05$). However, when $Ctns^{-/-}$ mice ($n = 10$) were placed in the open-field enclosure, they were less active than their wild-type ($n = 8$) and heterozygous littermates ($n = 5$). Total activity, corresponding to the total number of squares crossed, was significantly lower in $Ctns^{-/-}$ mice (117.8 ± 39.2) than in $Ctns^{+/+}$ (247.9 ± 40.7; $P = 0.03$) and $Ctns^{+/-}$ (296.3 ± 33.1; $P = 0.009$) mice. Circumference activity (54.5 ± 17.9 versus 117.4 ± 18.9 [$P = 0.02$]; 134.2 ± 17.3 [$P = 0.01$]) and the number of rearing behaviors (3.8 ± 2.3 versus 24 ± 8 [$P = 0.04$]; 37 ± 7.1 [$P = 0.001$]) were also significantly decreased. Moreover, $Ctns^{-/-}$ mice had a delayed onset of movement and tended to walk backwards and along the walls.

Muscle and bone analyses. CPK levels were higher in $Ctns^{-/-}$ ($n = 34$) mice than in $Ctns^{+/+}$ ($n = 12$) mice but the difference was not significant ($1,715 \pm 597$ versus 809 ± 126 IU/liter; $P > 0.05$). Interestingly, 4 $Ctns^{-/-}$ mice showed significantly higher CPK levels, greater than 3,000 IU/liter.

X-ray examination of 3 $Ctns^{-/-}$ and 3 $Ctns^{+/+}$ mice (two 6 months old and four 9 months old) showed a decrease in bone mineralization and in cortical width along the diaphysis in the $Ctns^{-/-}$ mice, compared to the wild-type mice (Fig. 5a and b). Moreover, a bone deformity was particularly visible along the tibia and femurs in a 9-month-old $Ctns^{-/-}$ mouse (Fig. 5a). Histological sections of the tibiae of $Ctns^{-/-}$ mice showed marked osteoporosis characterized by thinning of the compact bone of the diaphysis and a decrease in the mass of the epiphysis spongy bone, as shown by comparison with $Ctns^{+/+}$ mice (Fig. 5c and d).
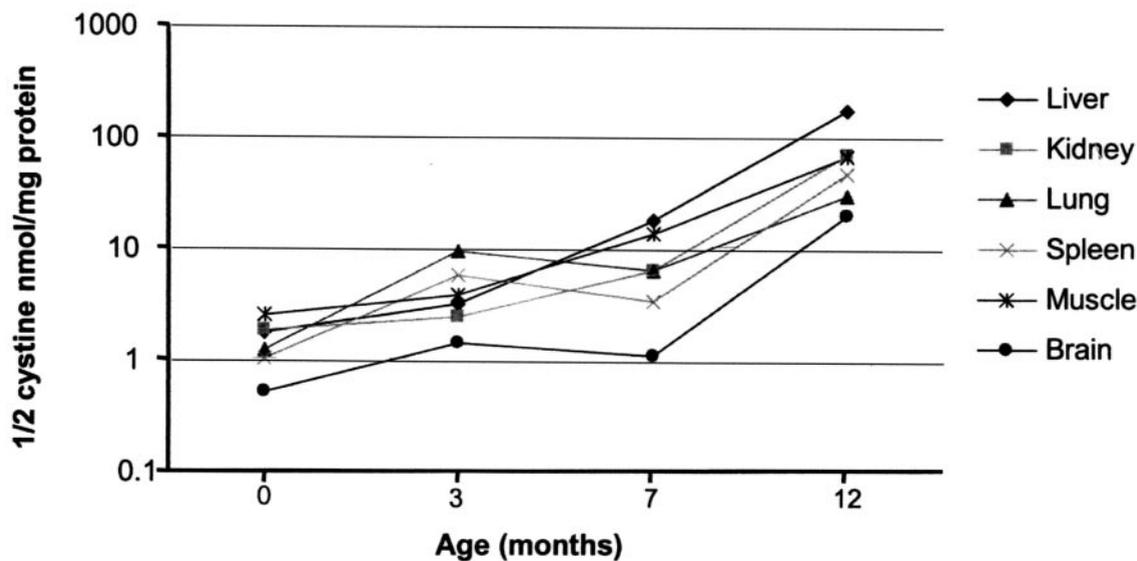
a
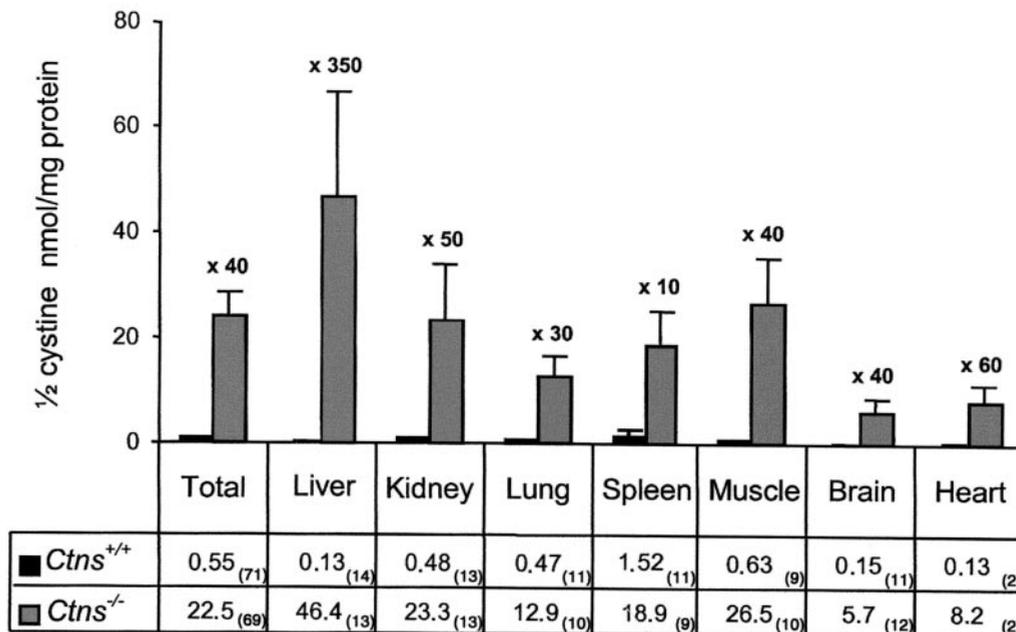
b

FIG. 3. Intracellular cystine content (measured as nanomoles of half-cystine per milligram of protein) of various organs. (a) A total of 140 assays were performed, 71 on $Ctns^{+/+}$ mice (black bars) and 69 on $Ctns^{-/-}$ mice (gray bars), from birth to 1 year of age. The cystine content of all tissues of $Ctns^{-/-}$ mice was significantly increased in comparison to that observed in their wild-type littermates. The number of mice assayed for each tissue is indicated in parentheses. Error bars correspond to the SEM. (b) Graph showing the increase in cystine content of all organs of $Ctns^{-/-}$ mice with respect to age (semilogarithmic).

Ocular examination. The global retinal function of $Ctns^{-/-}$ mice was determined using ERG responses. Two 8-month-old $Ctns^{-/-}$ mice of the 4 studied gave abnormal scotopic and photopic responses in comparison to the C57Bl/6 controls.

One of these mice ($Ctns^{-/-}$ A) gave an excessive ERG profile previously reported as "supernormal" (12), with the amplitude being clearly increased in comparison to the controls (Fig. 6a). In contrast, for the other ($Ctns^{-/-}$ B), the ERG profile was
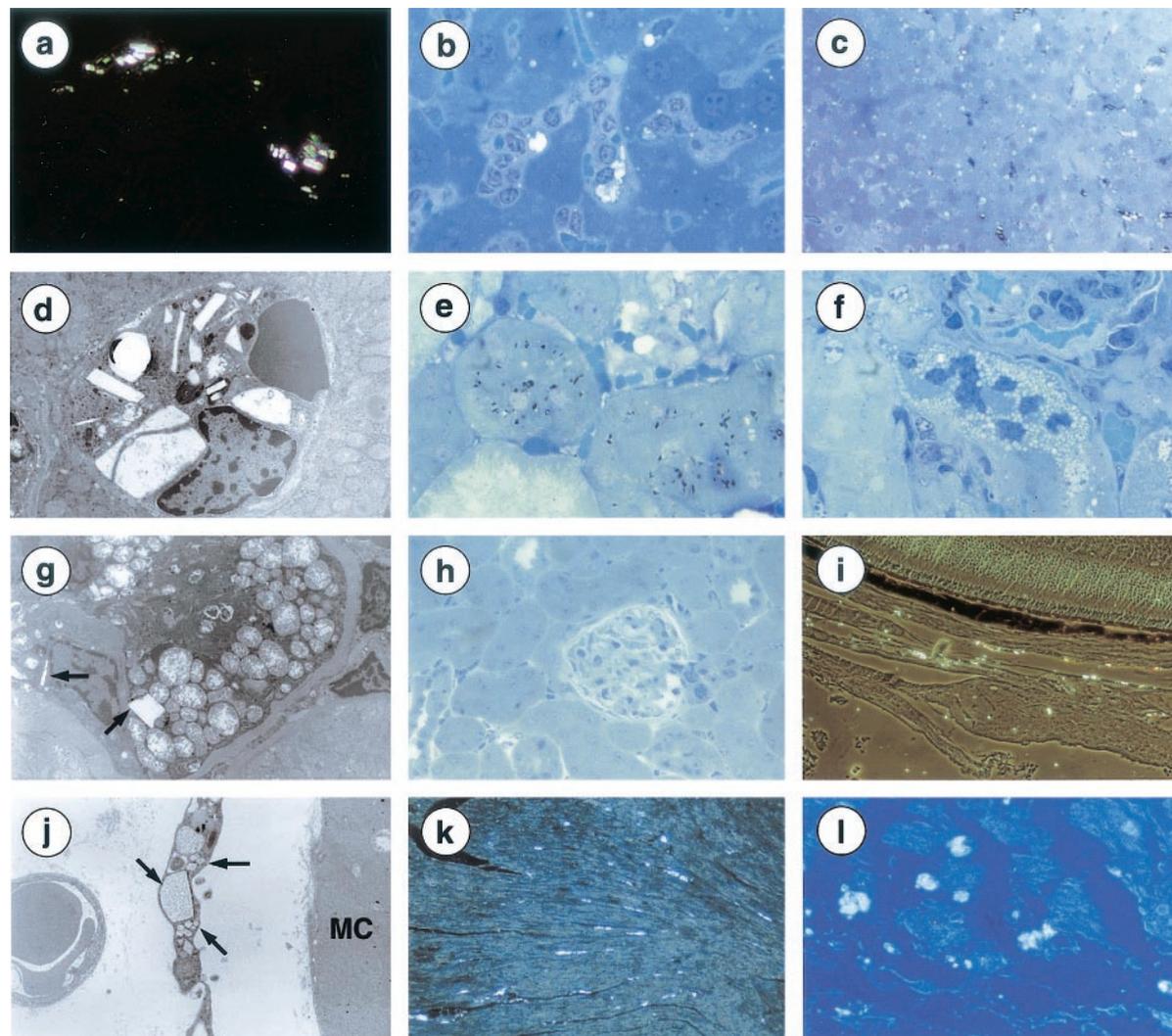
FIG. 4. Histological findings in *Ctns*$^{-/-}$ mice. (a) Refractive rectangular white cystine crystals within interstitial cells of the renal capsule (18-month-old mouse). Magnification, ×400. (b) Cystine crystal in Küpffer cells. Hepatocytes are preserved (35-week-old mouse). Magnification, ×750. (c) Dark staining of several Küpffer cells, some of them containing crystals (35-week-old mouse). Magnification, ×320. (d) Crystals of various sizes and shapes within a Küpffer cell (1-year-old mouse). Magnification, ×2,750. (e) Dark inclusions within proximal tubular cells (35-week-old mouse). Magnification, ×750. (f) Focal microvacuolization of proximal tubular cells (35-week-old mouse). Magnification, ×750. (g) Swollen mitochondria with clear matrix and disorganized cristae. Rare crystals (arrows) (1-year-old mouse). Magnification, ×2,000. (h) Normal renal parenchyma (1-year-old mouse). Magnification, ×320. (i) Abundant crystals in the choroid, but not in the retina (1-year-old mouse). Magnification, ×320. (j) Skeletal muscle: crystals in interstitial cells (arrows) but not in myocytes (MC) (1-year-old mouse). Magnification, ×4,400. (k) Heart. Crystals in the left ventricle (1-year-old mouse). Magnification, ×200. (l) Heart. Crystals in the atria (1-year-old mouse). Magnification, ×320. (a, c, h, and l) Formol fixation, paraffin embedding, phase contrast microscopy. (b, f, and h) Glutaraldehyde fixation, epoxy resin embedding, semithin section, toluidine blue staining. (c and e) Osmium tetraoxide fixation, epoxy resin embedding, semithin section, toluidine blue staining. (d, g, and j) Electron microscopy, glutaraldehyde fixation, epoxy resin embedding, lead citrate, and uranyl acetate staining.

severely impaired showing a reduced amplitude (Fig. 6a). Slit lamp examination of the four *Ctns*$^{-/-}$ mice detected the presence of cystine crystals in the cornea (Fig. 6b), and funduscopic examination showed patches of depigmentation in the peripheral retina of the *Ctns*$^{-/-}$ mouse with the impaired ERG (Fig. 6c); these abnormalities were not seen in the two controls.

Therapeutic cysteamine trial. The cystinosis mouse model was used to test the effectiveness of cystine clearance by cysteamine (Cystagon; Orphan Europe, Paris, France) in various tissues. The drug was administered in a water bottle and prepared fresh each day. We treated three *Ctns*$^{-/-}$ mice with

cysteamine at 200 or 400 mg/kg of body weight and sequentially sacrificed them 7 and 30 days after treatment with 200 mg/kg and 60 days after with 400 mg/kg. With the 200-mg/kg treatment, a decrease in cystine content was observed after 7 days, becoming more significant after 30 days (data not shown). The most notable result, however, was observed following a 60-day treatment with the 400-mg/kg dose, showing a clear decrease in the cystine levels of all tissues tested with variable efficiency: a decrease of 77% was seen in the liver (16.92 versus 4.93), 50% in the kidney (6.14 versus 3.16), 49% in the lung (5.99 versus 3.10), 13% in the spleen (3.21 versus 2.79), 52% in the muscle
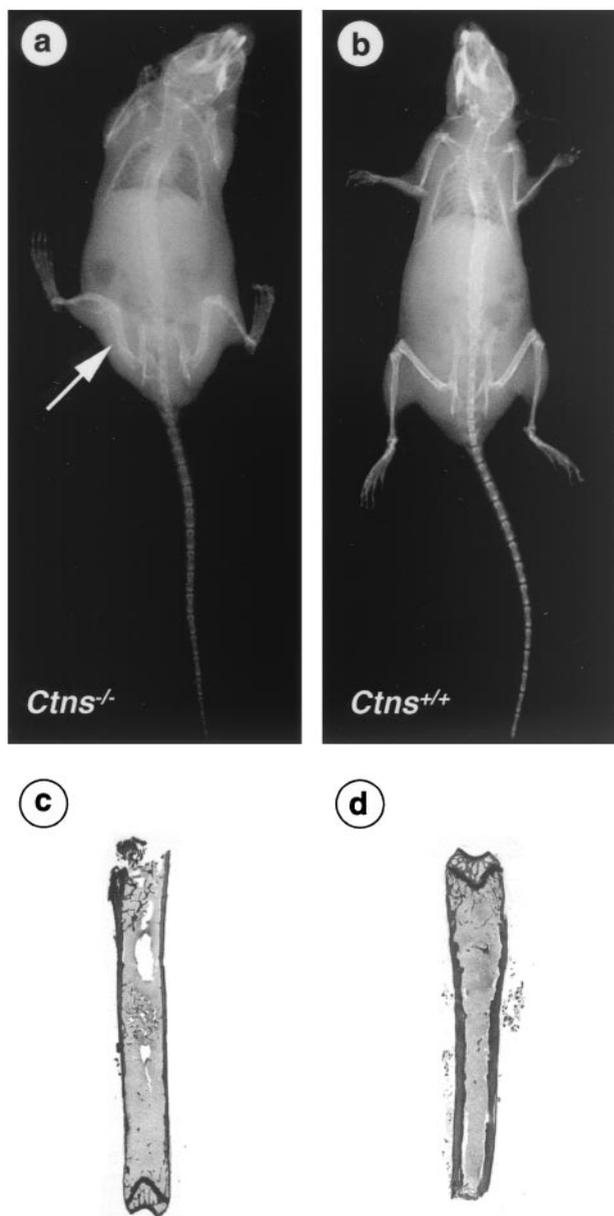
FIG. 5. Bone X-ray and histological examination. X-rays of a *Ctns*⁻/⁻ (a) and a *Ctns*⁺/⁺ (b) mice. A decrease in bone density and cortical width along the diaphysis can be seen in the *Ctns*⁻/⁻ mouse. Moreover, bone deformity is particularly visible on the tibia and femurs (arrow). Histological sections of a *Ctns*⁻/⁻ (c) and *Ctns*⁺/⁺ (d) mice confirm the thinning of the compact bone of the diaphysis.

(13.39 versus 6.35), and 34% in the brain (0.65 versus 0.43). Cystine levels were not reduced to wild-type levels following treatment.

DISCUSSION

We report here the generation of the first known animal model for cystinosis. We replaced the last four exons of the murine *Ctns* gene, which encode the last five TM, by an IRES-β*gal-neo* cassette, using homologous recombination. The targeting strategy chosen for modifying *Ctns* was modeled on the site of mutations in individuals with nephropathic cystinosis. Affected individuals carrying point mutations in the sequences encoding the last three TM of cystinosin have a phenotype clinically indistinguishable from that of individuals in whom the entire gene is deleted (2). Thus, a gene-targeting event that interrupted the protein before the third TM was judged sufficient to completely disrupt the function of the protein. We verified by subcellular localization and functional studies that murine cystinosin shares the same characteristics than human cystinosin and that the truncated cystinosin is clearly not localized to lysosomes and has lost its cystine transport function, confirming the lack of production of a functional cystinosin, should the truncated protein be stable, from the recombinant allele in the *Ctns*⁻/⁻ mice. Thus, a residual function of cystinosin cannot account for the phenotype observed in *Ctns*⁻/⁻ mice (cf. infra).

Ctns⁻/⁻ mice accumulated cystine in all tissues tested, and cystine levels increased with age. However, cystine content differed significantly between tissues, as has also been reported for the few human cystinotic tissues tested (17). Comparisons between the tissue cystine content of *Ctns*⁻/⁻ mice and affected individuals are difficult given this small number of human tissues tested and experimental variability. However, a loose comparison can be made with regard to the level of increase. For example, in liver, kidney, and muscle, cystine levels increased by factors of 1,350, 413, and 120, respectively, for the oldest mice assayed (1 year old). These values fall into the range reported for humans, which are a 50- to 9,000-fold increase in the liver, a 175- to 380-fold increase in the kidney, and a 33- to 567-fold increase in muscle (17), demonstrating comparable levels of cystine storage and intertissue variability in the two species. Surprisingly, although *Ctns* is faintly expressed in normal mouse muscle as showed by RT-PCR, inactivation of the *Ctns* gene clearly leads to cystine accumulation in muscle.

The kidney is one of the organs showing the highest levels of cystine accumulation. Despite this cystine accumulation, the *Ctns*⁻/⁻ mice present no signs of proximal tubulopathy, even at 18 months of age. This observation is surprising because the proximal tubular defect appears as early as 6 months in children with infantile cystinosis (17). In addition, the *Ctns*⁻/⁻ mice do not present the severe and diffuse proximal tubule alterations seen in humans (19). They have only very focal cystine crystal deposits within proximal tubular cells, a finding rarely reported in patients (24). The early onset of the proximal tubulopathy observed in affected children is unique among the other clinical signs of cystinosis, most of which appear later when a massive accumulation of cystine crystals is present (17). This observation suggests that the proximal tubulopathy seen in humans may be a secondary metabolic consequence rather than a direct effect of cystine storage. Along this line, previous studies have shown that the lysosomes of cystine-loaded rabbit proximal tubules display a significant reduction in intracellular ATP concentrations, leading to inhibition of NaK-ATPase activity (10). This defect would decrease the gradient for sodium entry into the tubular cells and thus reduce the sodium-coupled transport of other solutes. These data suggest that the mitochondrial oxidative phosphorylation process responsible for ATP synthesis is impaired in cystinosis proximal tubular cells. Consistently, large mitochondria are focally observed in
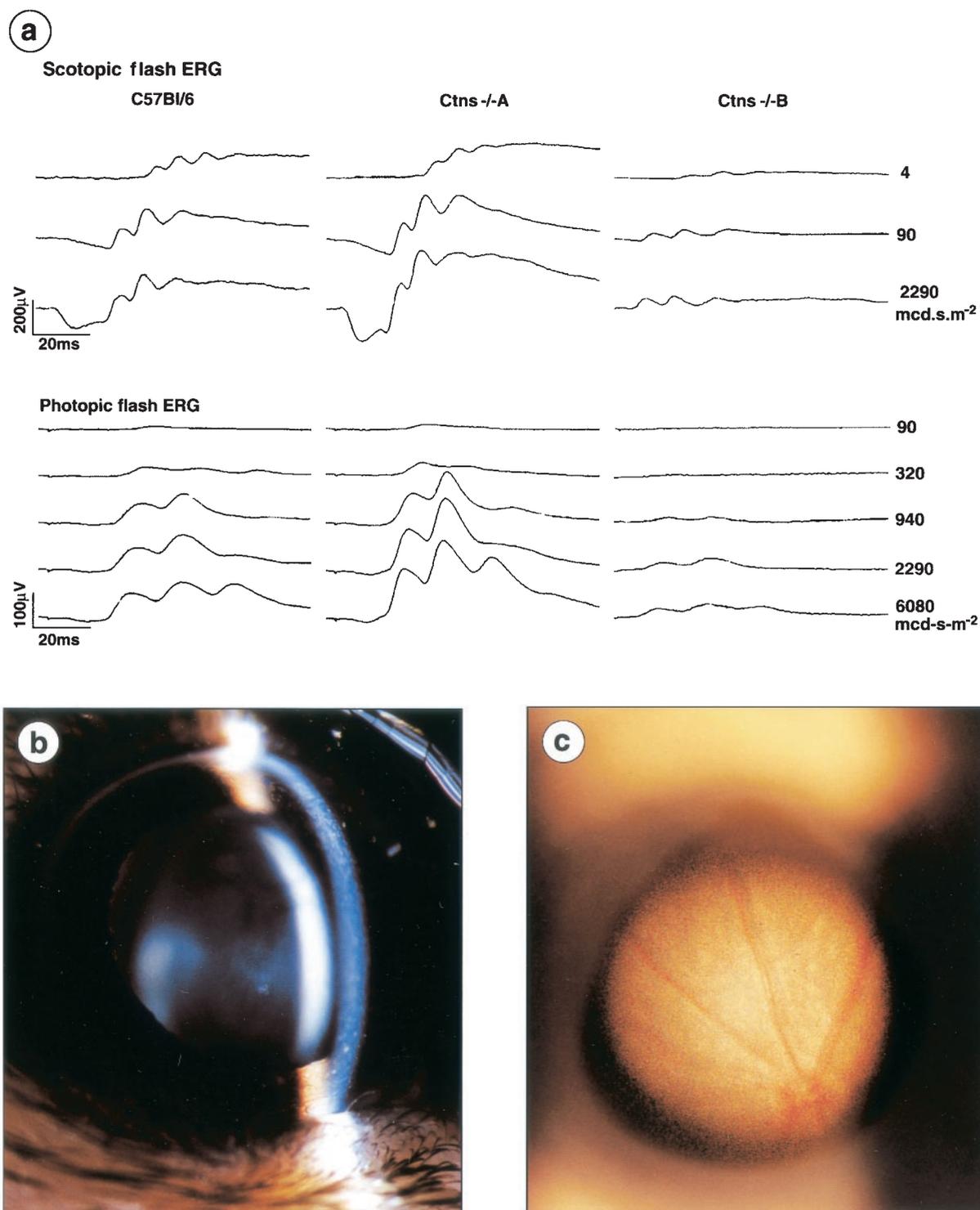
FIG. 6. Ocular examination. (a) Electroretinograms of 2 $Ctns^{-/-}$ mice and a control C57BL/6 mouse. The $Ctns^{-/-}$ mouse A presents a supernormal ERG, the amplitude is increased for the scotopic and photopic responses. For the $Ctns^{-/-}$ mouse B, the amplitude is severely impaired for both responses. (b) Slit lamp photography of the cornea of a $Ctns^{-/-}$ mouse. Cystine crystals, consisting of fine white, needle-shaped points, can be observed in the cornea. (c) Funduscopic photography of the retina of a $Ctns^{-/-}$ mouse. Patches of depigmentation are seen in the peripheral retina.

the proximal tubular cells of $Ctns^{-/-}$ mice, and mitochondrial swelling has been described in kidney biopsies from cystinotic patients (21, 29). Thus, the lack of tubulopathy in $Ctns^{-/-}$ mice might be accounted for by the existence of an alternative pathway that rescues ATP depletion in murine proximal tubular cells.

Cystine crystals were observed in the interstitial cells and macrophages of most organs of $Ctns^{-/-}$ mice, as reported for cystinotic individuals (5). The moderate cystine crystal accumulation in the $Ctns^{-/-}$ mice, compared to that observed in human patients, appears to remain stable from 8 to 18 months without severe consequences. Less-severe phenotypes in mouse models than in humans have also been described in other lysosomal storage diseases. For example, the α-glucosidase knockout mouse, a model of Pompe disease, accumulates glycogen in the lysosomes of heart, liver and muscle, but only presents mild cardiomegaly. In contrast, affected children die before 2 years of age due to severe cardiomyopathy (4). The authors suggested that the life span of mice may be insufficient for the development of the clinical symptoms of lysosomal storage diseases seen in humans. This hypothesis may also hold true for the cystinosis mouse model with regard to the late clinical signs of cystinosis. An alternative hypothesis, could be the existence of a passive efflux of cystine from the mouse lysosomes. The lysosomal cystine transporter studied in mouse L-929 fibroblasts (18) has the same characteristics as human cystinosin (22). However, it was postulated that a nonsaturable pathway for cystine efflux may exist in mouse lysosomes (18). If such a pathway exists in mouse and not in humans, it may act to keep cystine levels below the critical threshold for the appearance of the clinical signs associated with cystinosis.

In contrast, the ocular abnormalities observed in $Ctns^{-/-}$ mice are similar to those reported in cystinotic children. Corneal cystine crystal deposits were detected in all the four 8-month-old $Ctns^{-/-}$ mice by slit lamp examination. They are pathognomonic (12) and virtually constant at the age of 1 year in cystinotic patients (11). The ERG was normal in two $Ctns^{-/-}$ mice, "supernormal" in one, and impaired in the other. These results are similar to those reported in a study of 12 cystinotic patients (normal ERG in six, supernormal in three, and flat in three) (12). The supernormal ERG may result from the dispersion of light by the refractile crystals in the cornea (Tyndall's effect), which could produce stronger retinal stimuli and increase the ERG response. Conversely, the severely impaired ERG correlates with the retinopathy observed in affected individuals from as early as three years of age (11). This retinopathy is characterized by patches of depigmentation in the peripheral retina, which can extend to the macula, leading to decrease in visual acuity (12). Such patches of depigmentation were observed in the $Ctns^{-/-}$ mouse with an impaired ERG. These results strongly suggest that $Ctns^{-/-}$ mice also have altered visual functions, which could lead to blindness in time, as for cystinotic individuals.

This hypothesis could account for the behavioral anomalies in these mice that appear around six months. $Ctns^{-/-}$ mice showed a reduced motility in comparison to their wild-type littermates, as indicated by their performance in the open-field test, which represents an unknown and potentially dangerous environment (35). A lack of movement at the beginning of the test, continual wall hugging, and a reduction in overall activity

are indicative of anxiety in the $Ctns^{-/-}$ mice (9). Another explanation for behavioral abnormalities could be neurological and/or muscular defects. In cystinotic patients, encephalopathy has been reported from 15 years of age (6), and cystine crystals detected in all portions of the central nervous system (17). Myopathy has been described in young adults (17), and cystine crystals reported within cells adjacent to the myocytes (15). This cystine accumulation could lead to fiber atrophy or necrosis (36). In $Ctns^{-/-}$ mice, cystine crystals were not detected in the brain, but they were observed in muscle interstitial cells and associated with foci of myocyte necrosis in one of the four $Ctns^{-/-}$ mice studied. CPK levels were also significantly higher in some $Ctns^{-/-}$ mice. Taken together, these results may indicate the presence of muscular abnormalities in some of the $Ctns^{-/-}$ mice. The fact that only a few mice so far show any indication of such anomalies, correlates with the small proportion of myopathy cases observed among cystinosis patients (33).

This phenotypic variability, observed both for muscle and retinal abnormalities, may be explained by the fact that the mice are from mixed genetic backgrounds. We are currently crossing the $Ctns^{-/-}$ mice onto several pure genetic backgrounds in order to obtain homogeneous genotypes which would likely lead to more reproducible phenotypes.

Finally, we observed a bone demineralization and cortical thinning of vertebrae and long bones of $Ctns^{-/-}$ mice. In cystinotic children, bone abnormalities are a consequence of hypophosphatemic rickets and hyperparathyroidism secondary to renal failure (17). As this cannot be the cause in the knockout mice, the observed bone defects may be a direct consequence of cystine storage, as observed in other lysosomal storage disease. For example, diffuse osteoporosis is a common feature observed in Gaucher's disease caused by increased osteoclast activation due to glucosylceramide storage in cells (3). A bone defect due to cystine storage may also partially explain the poor growth of cystinotic children, which is more severe than for children with a tubulopathy or renal failure from other etiologies, and which seems to be partially improved with cysteamine therapy (17).

Preliminary therapeutic trials using an oral administration of cysteamine, even performed only with a few number of animals, allowed us to demonstrate the efficiency of this treatment for cystine clearance in $Ctns^{-/-}$ mice. An obvious decrease was observed in all tissues tested, although cystine levels were not reduced to control wild-type levels. The depletion of lysosomal cystine concentrations in cysteamine-treated patients is also partial (14, 16). A more thorough therapeutic trial should now be carried out in $Ctns^{-/-}$ mice, with cysteamine administration beginning at birth, to correctly evaluate the capacity of this drug to reduce cystine content in various tissues and prevent the appearance of clinical signs.

In conclusion, the $Ctns^{-/-}$ mouse model could prove to be a valuable model for cystinosis. Elevated cystine levels, and the distribution of cystine crystals, in the knockout mice are comparable to those in affected individuals. However, cystine crystal accumulation in $Ctns^{-/-}$ mice is moderate in comparison to that in cystinotic individuals, and the phenotype of these mice is less severe than that observed for patients with infantile cystinosis. The $Ctns^{-/-}$ mice do, however, present with ocular abnormalities similar to those observed in affected individuals

and with a bone defect that may help explain the severity of the bone disease of cystinotic children. The lack of proximal tubulopathy in the *Ctns*$^{-/-}$ mouse constitutes a major difference from the infantile form of the disease. Thus, the comparison of the two species may bring to light the cause of the proximal tubulopathy seen in children with cystinosis, the exact origin of which remains a major question. Finally, this animal model is an essential and unique tool for testing the ability of emerging therapies to reduce cystine levels and for comparing their efficiency with that of the treatment currently in use.

REFERENCES

1. **Anikster, Y., C. Lucero, J. Guo, M. Huizing, V. Shotelersuk, I. Bernardini, G. McDowell, F. Iwata, M. I. Kaiser-Kupfer, R. Jaffe, J. Thoene, J. A. Schneider, and W. A. Gahl.** 2000. Ocular nonnephropatic cystinosis: clinical, biochemical, and molecular correlations. Pediatr. Res. **47:**17–23.
2. **Attard, M., G. Jean, L. Forestier, S. Cherqui, W. van't Hoff, M. Broyer, C. Antignac, and M. Town.** 1999. Severity of phenotype in cystinosis varies with mutations in the CTNS gene: predicted effect on the model of cystinosin. Hum. Mol. Genet. **8:**2507–2514.
3. **Barak, V., M. Acker, B. Nisman, I. Kalickman, A. Abrahamov, A. Zimran, and S. Yatziv.** 1999. Cytokines in Gaucher's disease. Eur. Cytokine Netw. **10:**205–210.
4. **Bijvoet, A. G., E. H. van de Kamp, M. A. Kroos, J. H. Ding, B. Z. Yang, P. Visser, C. E. Bakker, M. P. Verbeet, B. A. Oostra, A. J. Reuser, and A. T. van der Ploeg.** 1998. Generalized glycogen storage and cardiomegaly in a knockout mouse model of Pompe disease. Hum. Mol. Genet. **7:**53–62.
5. **Broyer, M., M. Guillot, M. C. Gubler, and R. Habib.** 1981. Infantile cystinosis: a reappraisal of early and late symptoms. Adv. Nephrol. Necker Hosp. **10:**137–166.
6. **Broyer, M., M. J. Tete, G. Guest, J. P. Bertheleme, F. Labrousse, and M. Poisson.** 1996. Clinical polymorphism of cystinosis encephalopathy. Results of treatment with cysteamine. J. Inherit. Metab. Dis. **19:**65–75.
7. **Cherqui, S., V. Kalatzis, G. Trugnan, and C. Antignac.** 2001. The targeting of cystinosin to the lysosomal membrane requires a tyrosine-based signal and a novel sorting motif. J. Biol. Chem. **276:**13314–13321.
8. **Cherqui, S., V. V. Kalatzis, L. Forestier, I. I. Poras, and C. Antignac.** 2000. Identification and characterisation of the murine homologue of the gene responsible for cystinosis, Ctns. BMC Genomics **1:**2.
9. **Choleris, E., A. W. Thomas, M. Kavaliers, and F. S. Prato.** 2001. A detailed ethological analysis of the mouse open field test: effects of diazepam, chlordiazepoxide and an extremely low frequency pulsed magnetic field. Neurosci. Biobehav. Rev. **25:**235–260.
10. **Coor, C., R. F. Salmon, R. Quigley, D. Marver, and M. Baum.** 1991. Role of adenosine triphosphate (ATP) and NaK ATPase in the inhibition of proximal tubule transport with intracellular cystine loading. J. Clin. Invest. **87:**955–961.
11. **Dufier, J. L.** 1992. Ophthalmologic involvement in inherited renal disease. Adv. Nephrol. Necker Hosp. **21:**143–156.
12. **Dufier, J. L., P. Dhermy, M. C. Gubler, M. F. Gagnadoux, and M. Broyer.** 1987. Ocular changes in long-term evolution of infantile cystinosis. Ophthalmic Paediatr. Genet. **8:**131–137.
13. **Gahl, W. A., N. Bashan, F. Tietze, I. Bernardini, and J. D. Schulman.** 1982. Cystine transport is defective in isolated leukocyte lysosomes from patients with cystinosis. Science **217:**1263–1265.
14. **Gahl, W. A., L. Charnas, T. C. Markello, I. Bernardini, K. G. Ishak, and M. C. Dalakas.** 1992. Parenchymal organ cystine depletion with long-term cysteamine therapy. Biochem. Med. Metab. Biol. **48:**275–285.
15. **Gahl, W. A., M. C. Dalakas, L. Charnas, K. T. Chen, G. H. Pezeshkpour, T. Kuwabara, S. L. Davis, R. W. Chesney, J. Fink, and H. T. Hutchison.** 1988. Myopathy and cystine storage in muscles in a patient with nephropatic cystinosis. N. Engl. J. Med. **319:**1461–1464.
16. **Gahl, W. A., G. F. Reed, J. G. Thoene, J. D. Schulman, W. B. Rizzo, A. J. Jonas, D. W. Denman, J. J. Schlesselman, B. J. Corden, and J. A. Schneider.** 1987. Cysteamine therapy for children with nephropatic cystinosis. N. Engl. J. Med. **316:**971–977.
17. **Gahl, W. A., J. Thoene, and J. A. Schneider.** 2001. Cystinosis: a disorder of lysosomal membrane transport, p. 5085–5108. *In* C. R. Scriver, A. L. Beaudet, W. S. Sly, and D. Valle (ed.), The metabolic and molecular bases of inherited disease, 8th ed., vol. 3. McGraw Hill, New York, N.Y.
18. **Greene, A. A., E. G. Marcusson, G. P. Morell, and J. A. Schneider.** 1990. Characterization of the lysosomal cystine transport system in mouse L-929 fibroblasts. J. Biol. Chem. **265:**9888–9895.
19. **Gubler, M. C., M. Lacoste, M. Sich, and M. Broyer.** 1999. The pathology of the kidney in cystinosis, p. 42–48. *In* M. Broyer (ed.), Cystinosis. Elsevier, Paris, France.
20. **Hogan, B., R. Beddington, F. Costantini, and E. Lacy.** 1994. Manipulating the mouse embryo, 2nd ed. Cold Spring Harbor Laboratory Press, Cold Spring Harbor, New York.
21. **Jackson, J. D., F. G. Smith, N. N. Litman, C. L. Yuile, and H. Latta.** 1962. The Fanconi syndrome with cystinosis. Electron microscopy of renal biopsy specimens from five patients. Am. J. Med. **33:**893–910.
22. **Kalatzis, V., S. Cherqui, C. Antignac, and B. Gasnier.** 2001. Cystinosin, the protein defective in cystinosis, is a H$^+$-driven lysosomal cystine transporter. EMBO. J. **20:**5940–5949.
23. **Lowry, O. H., N. J. Rosebrough, A. L. Farr, and R. J. Randall.** 1951. Protein measurement with the folin phenol reagent. J. Biol. Chem. **193:**265–275.
24. **Mahoney, C. P., and G. E. Striker.** 2000. Early development of the renal lesions in infantile cystinosis. Pediatr. Nephrol. **15:**50–56.
25. **Oshima, R. G., R. C. Willis, C. E. Furlong, and J. A. Schneider.** 1974. Binding assay for amino acids. The utilization of a cystine binding protein from Escherichia coli for the determination of acid-soluble cystine in small physiological samples. J. Biol. Chem. **249:**6033–6039.
26. **Peachey, N. S., L. Roveri, A. Messing, and M. A. McCall.** 1997. Functional consequences of oncogene-induced horizontal cell degeneration in the retinas of transgenic mice. Vis. Neurosci. **14:**627–632.
27. **Pellett, O. L., M. L. Smith, A. A. Greene, and J. A. Schneider.** 1988. Lack of complementation in somatic cell hybrids between fibroblasts from patients with different forms of cystinosis. Proc. Natl. Acad. Sci. USA **85:**3531–3534.
28. **Schneider, J. A., K. Bradley, and J. E. Seegmiller.** 1967. Increased cystine in leukocytes from individuals homozygous and heterozygous for cystinosis. Science **157:**1321–1322.
29. **Spear, G. S., R. J. Slusser, A. J. Tousimis, C. G. Taylor, and J. D. Schulman.** 1971. Cystinosis. An ultrastructural and electron-probe study of the kidney with unusual findings. Arch. Pathol. **91:**206–221.
30. **Thoene, J., R. Lemons, Y. Anikster, J. Mullet, K. Paelicke, C. Lucero, W. Gahl, J. Schneider, S. G. Shu, and H. T. Campbell.** 1999. Mutations of CTNS causing intermediate cystinosis. Mol. Genet. Metab. **67:**283–293.
31. **Town, M., G. Jean, S. Cherqui, M. Attard, L. Forestier, S. A. Whitmore, D. F. Callen, O. Gribouval, M. Broyer, G. P. Bates, W. van't Hoff, and C. Antignac.** 1998. A novel gene encoding an integral membrane protein is mutated in nephropatic cystinosis. Nat. Genet. **18:**319–324.
32. **Vallet, V. S., A. A. Henrion, D. Bucchini, M. Casado, M. Raymondjean, A. Kahn, and S. Vaulont.** 1997. Glucose-dependent liver gene expression in upstream stimulatory factor 2 −/− mice. J. Biol. Chem. **272:**21944–21949.
33. **Vester, U., M. Schubert, G. Offner, and J. Brodehl.** 2000. Distal myopathy in nephropatic cystinosis. Pediatr. Nephrol. **14:**36–38.
34. **Voss, A. K., T. Thomas, and P. Gruss.** 1997. Germ line chimeras from female ES cells. Exp. Cell Res. **230:**45–49.
35. **Wilson, R. C., T. Vacek, D. L. Lanier, and D. A. Dewsbury.** 1976. Open-field behavior in muroid rodents. Behav. Biol. **17:**495–506.
36. **Wockel, W., W. Meerbach, and D. Rudiger.** 1971. Cystinosis with involvement of the central nervous system and muscles (myopathy). Zentbl. Allg. Pathol. **114:**493–498.